Application of Rice Husk Ash as Thermal Insulation Materials

Chee Wah Loy[1,2,*] (iD), Khamirul Amin Matori[2,3], M.M. Haslinawati[2], Mohd Hafiz Mohd Zaid[2,3], Norhazlin Zainnudin[4]

[1]School of Chemistry, The University of Sydney, Sydney NSW 2006, Australia
[2]Department of Physics, Universiti Putra Malaysia, 43400 UPM Serdang, Selangor, Malaysia
[3]Materials Synthesis and Characterization Laboratory, Institute of Advanced Technology, Universiti Putra Malaysia, 43400 UPM Serdang, Selangor, Malaysia
[4]Department of Chemistry, Universiti Putra Malaysia, 43400 UPM Serdang, Selangor, Malaysia

*Corresponding author: E-mail: chee.loy@sydney.edu.au

A low thermal diffusivity SiO_2-based ceramic was fabricated by sintering Malaysia agricultural waste rice husk at 800 °C. This paper presents the effect of sintering temperatures on the phase transformation, microstructure and thermal diffusivity of rice husk ash (RHA) as a thermal insulating material. A series of SiO_2-based ceramics were fabricated from rice husk *via* two sintering stages. Rice husk was pre-sintered at 700 °C and then ground into powder. The RHA powder was compacted into pellets and then re-sintered at a single temperature between 700 and 1400 °C. Sintering of the RHA induces phase transformation from amorphous silica to crystalline α-cristobalite, α-tridymite and β-tridymite. The thermal diffusivities of RHA were evaluated using the laser flash analysis technique. The results indicate RHA-800 °C has the lowest thermal diffusivity, which is 0.17 ± 0.1 mm^2 s^{-1} at 25 °C. The RHA particle morphologies were observed using a field-emission scanning electron microscopy. Low-frequency vibrational modes of silica such as lattice vibration were investigated using Fourier-transform infrared spectroscopy technique. X-ray fluorescence result indicated that RHA-800 °C contains ~90 *wt* % of SiO_2.

Introduction

Rice husk is an agro-waste from the rice milling process. It constitutes about ~20 % of weight paddy [1]. The main components in rice husk are hydrated silica, lignin and cellulose [2]. Combustion of rice husk produces rice husk ash (RHA) and 13 to16 MJ kg^{-1} of heat energy [3]. The heat energy can be utilised as fuel for power generation. RHA is composed mainly of ~90% reactive amorphous silica [1]. Hence, it can be utilised to produce silica fused glass, silica fume, purity silica, silicon carbide and silica nitride [2,4]. High-temperature sintering of rice husk (>700 ºC) can also produce RHA with crystalline phases such as α-cristobalite, α-tridymite β-cristobalite and β-tridymite [1,2]. The phase composition of RHA depends on its sintering temperature [1,4]. β-cristobalite is the most thermodynamically stable phase among the silica polymorphs [2].

RHA has a high chemical and thermal shock resistance, high pozzolanic reactivity, high mechanical strength and low thermal conductivity [4,5]. These characteristics allow RHA to be used as building construction materials, reinforcing agents, composite fillers and thermal insulators [4,6]. Silica-based glass, ceramics and composites have been widely used as thermal insulation materials in various industrial applications [7-9]. The thermal conductivity and thermal diffusivity of fused silica glass at room temperature are 1.38 W m^{-1} K^{-1} and 0.8 mm^2 s^{-1}, respectively [10]. As temperature increases from room temperature, the thermal diffusivity of silica glass decreases and almost constant (~0.69 mm^2 s^{-1}) at temperatures beyond ~400 °C [10,11].

Thermal diffusivity is a physical quantity which evaluates the thermal conductivity of a material per unit volumetric heat capacity [11]. It reflects the rate of heat transfer through a material. The thermal diffusivity is a temperature dependence [11]. The main heat carrier in ceramic materials is an elastic lattice vibrational wave called phonon [12]. Hence, the heat transport in ceramic materials is closely related to the phonon velocities and phonon mean free paths. Phonon scattering occurs when phonons interacted with other phonons, particle interfaces or phase boundaries. Phonons lose energy during the scattering process, which retards the rate of heat transfer. The microstructural characteristics of silica such as large crystalline grain size, low porosity, high purity and low particle dislocations can inhibit phonon scattering and increase the phonon mean free paths [5,7]. Therefore, amorphous and low crystallinity silica with a high specific surface area (*e.g.* silica foams) is widely used as high-temperature resistant, fire extinguishing and thermal insulating materials [13,14].

In this study, Malaysian agricultural waste rice husk was employed to fabricate SiO_2-based ceramics. The main purposes of the present work are to study the effects of

Advanced Materials Letters
www.vbripress.com/aml

IAAM®
Advancement of Materials to Global Excellence
www.iaamonline.com

sintering temperature on the crystalline phase formation, density, microstructure and thermal diffusivity of RHA. The crystallinity, density and microstructural properties of RHA were correlated with their thermal diffusity behaviour for the application of thermal insulation.

Experimental

Rice husk was provided by the BERNAS Sdn. Bhd., Tanjung Karang. The rice husk was washed with deionised water and then dried in an oven at 120 °C for 24 hours. Dry rice husk was pre-sintered at 700 °C for 3 hours using an electric furnace. During the pre-sintering process, atmospheric gas was continuously supplied to burnt off organic and volatile compounds from the rice husk. The product of pre-sintering was hand-ground into powder and sieved using a 400-mesh stainless-steel wire sieve to produce RHA powder with a dimension of ≤36 μm.

In order to study the phase transformation, thermal diffusity and microstructural properties of dense RHA samples, pre-sintered RHA powder was compacted into 12.0 mm cylinder-shaped pellets and then re-sintered at a single temperature between 700 and 1400 ℃ for 3 hours. The heating and cooling rates were programmed as $+10\,℃\,min^{-1}$ and $-2\,℃\,min^{-1}$, respectively. Each pellet was made by compressing 1.0 g of pre-sintered RHA powder with a uniaxial pressure of 30 MPa using a laboratory pellet press, a 12.0 mm pellet die and polyvinyl acetate binder. The products of sintering were characterised by energy-dispersive x-ray fluorescence (EDXRF), powder x-ray diffraction (PXRD), Fourier-transform infrared (FTIR), field-emission scanning electron microscope (FESEM) and laser flash analysis (LFA) techniques.

The re-sintered RHA powder was prepared by hand-grounding the sintered pellets and then sieved using the 400-mesh stainless-steel wire sieve. EDXRF measurements were performed on an EDX-720 Shimadzu spectrometer to determine the elemental composition of RHA powder, which has been re-sintered to 800 °C and subsequent cooling. The instrument utilised x-ray produced from a Rh-target x-ray tube. PXRD measurements were performed on a PANAalytical (Philips) X'Pert Pro PW3050/60 diffractometer. CuK_a radiation with a wavelength of 1.5418 Å was utilised to access x-ray diffraction within the Bragg angles, 2θ of 10° to 90°. FTIR measurements were performed on a Perkin Elmer Spectrum 100 Series spectrometer with Universal attenuated total reflectance (ATP) accessory. The measurements utilised mid-infrared with a wavenumber spectral range of 4000 to 280 cm^{-1} to access the infrared transmission spectrum within the spectral range.

Bulk densities of sintered RHA pellets were evaluated using the acetone displacement method. The expression involved is given as $\rho_s = \rho_a\,(m_s/m_a)$, where ρ_s, ρ_a, m_s and m_a represent the bulk density of the measuring sample, the density of acetone (0.784 g cm^{-3}), the mass of the sample and the mass of acetone displaced by the sample, respectively. The microstructure of RHA powder was

observed using a FEI Nova NanoSEM 30 Series microscope under a high vacuum. The microscope was operated with an electron accelerating voltage of 3.00 kV to acquired high-resolution FESEM images.

The thermal diffusivities of sintered RHA pellets were measured using the LFA technique [11]. The measurements were performed on a NETZSCH-LFA 457 micro-flash instrument. During the measurements, the front sample surface was irradiated by a laser pulse, whereas the infrared radiation emitted from the rear sample surface was measured. In order to improve sample emissivity, RHA pellets were polished and then coated by carbon. The time required for rear sample surface temperature to reach half of its maximum value, $\tau_{1/2}$ was measured and the thermal diffusity, α of the sample at particular temperature was evaluated using the expression of $\alpha = 1.388\,L^2\,/\,(\tau_{1/2})$, where, L represents the specimen thickness [11]. The thermal diffusity of each sample was measured at temperatures between 25 and 300 °C, respectively.

Results and discussion

Rice husk burns violently when pre-sintered at 700 °C. The RHA appears black in colour, brittle, high porosity and easy to grind into a fine powder. Re-sintering of the black RHA at ≥700 °C and subsequent cooling in an electronic furnace with atmospheric gas supply yielded white RHA. It is due to the decarbonisation of char at high-temperature. The white RHA was ground into powder, sieved and compacted into pellets. The pellets were re-sintered at a single temperature between 700 and 1400 °C. The chemical composition of the pellet after sintered at 800 °C was measured using EDXRF technique. The EDXRF result indicates that the main component in RHA is SiO_2, which contributes 89.57 ± 0.31 *wt*.% of the RHA weight (**Table 1**). Besides, The RHA also contains K_2O, Fe_2O_3, Al_2O_3, Na_2O, P_5O_{10}, TiO_2, CaO and MgO. The results are close to the findings that reported in the literature [1,4].

Table 1. Weight compositions of dense RHA after re-sintering at 800 ℃.

Compounds	Weight Percentage (wt.%)
SiO_2	89.57 ± 0.31
K_2O	1.65 ± 0.01
Fe_2O_3	1.43 ± 0.01
Al_2O_3	1.32 ± 0.01
Na_2O	1.15 ± 0.01
P_2O_5	1.04 ± 0.01
TiO_2	1.01 ± 0.01
CaO	0.77 ± 0.01
MgO	0.76 ± 0.01
Others	1.30 ± 0.01

Fig. 1 shows the PXRD patterns of RHA which are produced from dynamically sintering to different temperatures. The PXRD results for RHA-700 °C and RHA-800 °C show a continuous pattern with a broad

diffused hump within 18º < 2θ < 30º. It reveals both samples are amorphous silica materials. A diffraction peak with low intensity was observed in the PXRD pattern of RHA-900 °C at 2θ = 21.85º. It may be attributed to the diffraction peak from low crystalline α-cristobalite or α-tridymite phases. Two sets of diffraction peaks are found in the PXRD patterns for RHA-1000 to RHA-1300 °C. These peaks are well-fitted with the diffraction patterns of α-cristobalite and α-tridymite, respectively. The intensity of the diffraction peaks increased as sintering temperature increases from 1000 to 1400 °C, indicating both α-cristobalite and α-tridymite crystals growth further at a higher temperature. The PXRD pattern of RHA-1400 ℃ indicates the sample has α-cristobalite, α-tridymite and an additional β-tridymite phase.
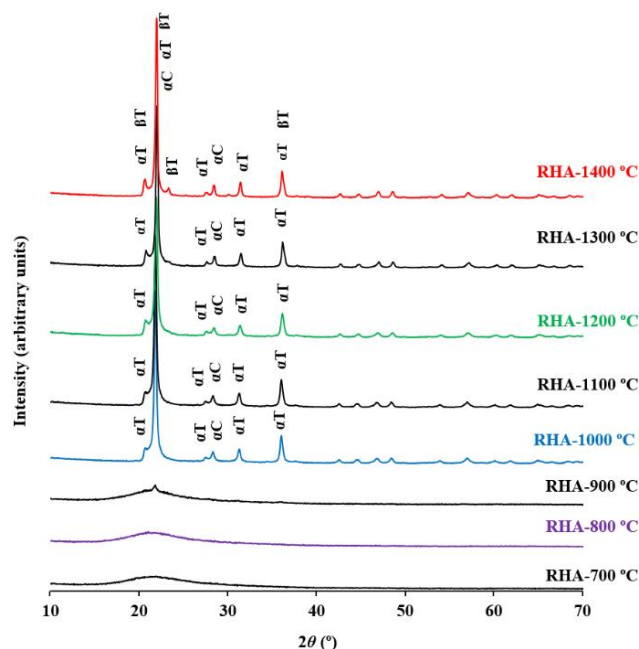
Fig. 1. PXRD patterns for RHA produced from the sintering at single temperature between 700 and1400 ℃, where αC = α-cristobalite; αT = α-tridymite; and βT = β-tridymite.

FTIR transmission spectra for sintered rice husk within the spectral range from 1600 to 280 cm^{-1} are shown in **Fig. 2**. There is no infrared absorption band between 4000 and 1400 cm^{-1}. All spectra have a broad infrared absorption band centered at ~1060 cm^{-1}. It corresponds to a common asymmetric Si–O–Si stretching vibrational mode of silica [2,13]. The products of sintering at 700, 800 and 900 °C have a similar FTIR spectrum. The infrared absorption bands at 799 and 452 cm^{-1} are attributed to the symmetric Si–O–Si stretching and bending vibrational modes of short-range ordered silica, respectively [2]. FTIR spectrum of RHA-1000 °C shows the infrared absorption band at 799 cm^{-1} shifted to 792 cm^{-1}, whereas the band at 450 cm^{-1} shifted to 472 cm^{-1}. These changes are associated with the vibrational modes of α-tridymite. Additional infrared absorption bands at 620, 380 and 300 cm^{-1} are attributed to lattice vibrational modes of α-cristobalite [15]. The infrared absorption band at 472 cm^{-1} also overlapped with the

O–Si–O bending and lattice vibrational modes of α-cristobalite [2]. The FTIR results are consistent with the PXRD findings.
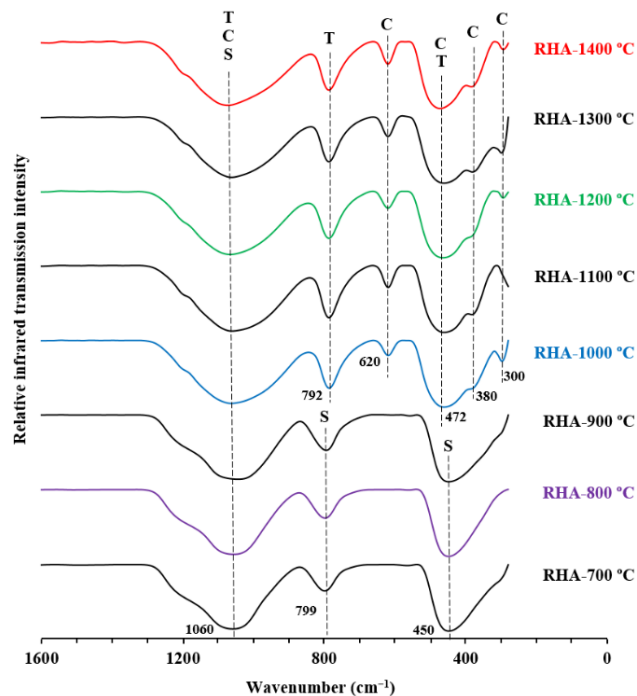

Fig. 2. FTIR transmission spectra for RHA produced from sintering at single temperature between 700 and1400 ℃, where S, C and T are correspond to the vibrational modes for short range ordered silica, tridymite and cristobalite, respectively.

The apparent densities for sintered RHA to various temperatures are shown in **Fig. 3**. The density of RHA increased gradually from 1.48 ± 0.1 to 1.55 ± 0.2 g cm^{-3} as sintering temperature varied from 800 to 1200 °C. The density of RHA increased rapidly to 1.69 ± 0.2 g cm^{-3} after sintering at 1400 °C. The densification of RHA is due to an increase in the kinetic energy of silica particles to realignment themselves into a denser structure.
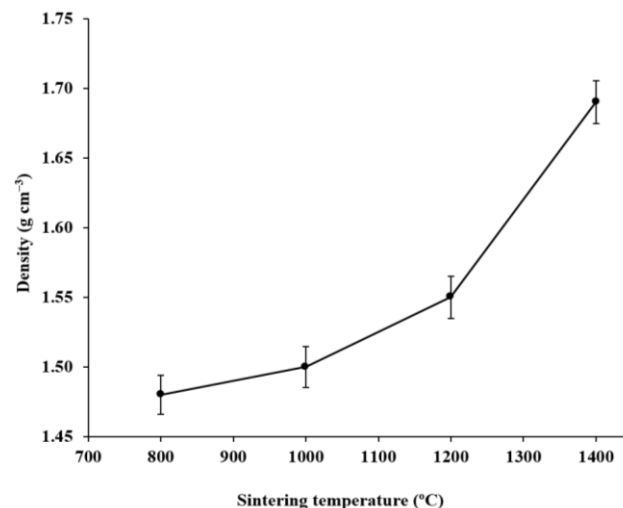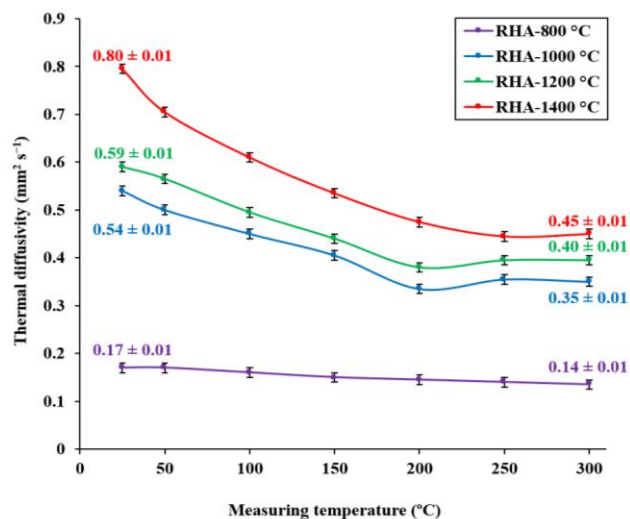

Fig. 3. Bulk densities for RHA produced from the sintering at 800, 1000, 1200 and 1400 ℃, respectively.
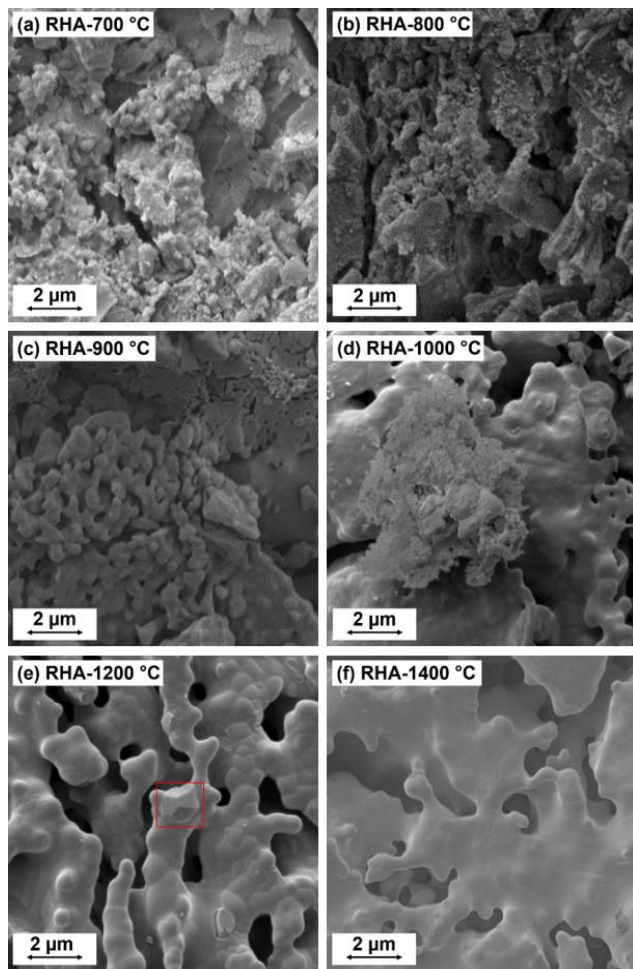
Fig. 4. FESEM micrographs for RHA produced from the sintering at (a) 700 °C, (b) 800 °C, (c) 900 °C, (d) 1000 °C, (e) 1200 °C and (f) 1400 °C, respectively.

The effects of sintering on the RHA particle surface were observed *via* FESEM. The surface microstructure of RHA after sintering at 700, 800, 900, 1000, 1200 and 1400 °C are presented in **Fig. 4 (a** to **f)**, respectively. In general, all RHA samples have a rough particle surface. The products of sintering at 700 and 800 °C are short-range ordered silica. They have a similar particle surface microstructure with no fractal pattern and high porosity. Sintering of rice husk at 900 and 1000 °C yielded RHA with a complex surface microstructure. There are more than one fractal patterns were observed from the FESEM micrographs. These fractal patterns reflect the growth of α-cristobalite or α-tridymite crystalline grains on an amorphous silica particle. The crystallisation of α-cristobalite and α-tridymite also produced pores with size <100 nm on silica particle surfaces. The sizes of crystalline grain and air pore are not well-defined from the FESEM micrographs because grains are connecting with no regular path length. The degree of connectivity between grains increased as sintering temperature increased from 900 to 1400 °C. The microstructure of RHA-1200 °C has the largest pore size compared to the products of sintering at other temperatures. A crystalline grain with a hexagonal

geometric was observed in the FESEM micrograph (**Fig. 4 (e)**). It is attributed to the α-tridymite, which has a hexagonal crystal system. RHA-1400 °C has a dense surface microstructure with no specific geometric and fractal patterns. As a result, it has the highest density $(1.69 \pm 0.2 \text{ g cm}^{-3})$ among other samples.

Fig. 5. Thermal diffusivity behaviours for RHA produced from the sintering at 800, 1000, 1200 and 1400 °C, respectively.

Fig. 5 shows the effects of the sintering of the thermal diffusivity behavior of RHA samples as a function of the measuring temperature. The RHA-800 °C sample is a highly disordered silica which has a lower thermal diffusivity compared to fused silica glass $(0.8 \text{ mm}^2.\text{s}^{-1})$ because the RHA-800 °C sample has low bulk density and highly porous structure [10]. The main heat carriers in amorphous silica are phonons [**12**]. The silica-pore interfaces in the highly porous RHA-800 °C sample induced phonon scattering, reduced phonon mean free paths and restrained phonon transport. Therefore, RHA-800 °C has the lowest thermal diffusivity $(0.17 \pm 0.1 \text{ mm}^2 \text{ s}^{-1})$ compared to other samples at 25 °C.

There is a substantial increase in the thermal diffusivity of RHA by increasing the sintering temperature of RHA from 800 to 1000 °C. This is associated with the phase transformation from amorphous silica to polycrystalline silica. The silica particles in the RHA-1000 °C are well-aligned in a longer-range order. They formed larger crystalline grains with a smaller grain interfacial area per unit volume. These features extended the phonon mean free and reduced the frequency of phonon scattering on particle interfaces. Hence, the RHA-1000 °C sample has a greater tendency to transport heat *via* lattice vibrations.

The thermal diffusivity of RHA-1200 °C is slightly higher than RHA-1000 °C. This is due to the RHA-1200 °C has a denser particle surface microstructure, larger grain size, higher bulk density and crystallinity. Greater increment in thermal diffusivity was observed as the sintering temperature of RHA from 1200 to 1400 °C. It is associated with to the densification and crystallisation of

β-tridymite, which has a higher thermodynamically stability. As a result, the RHA-1400 ℃ sample has the highest thermal diffusivity $(0.80 \pm 0.1 \text{ mm}^2 \text{ s}^{-1})$ among all samples.

The energy of phonons is a temperature-dependent parameter. As measuring temperature increases, a greater amount of heat energy was transported in the RHA sample *via* phonons. This also led to a greater amount of energy dissipated from phonon-phonon scattering. The thermal diffusivity of RHA is strongly affected by the rate of phonon energy gained from heat and the rate of phonon energy dissipated from phonon-phonon scattering at the instantaneous temperature. Since the phonon energy gained-to-energy dissipated ratio decreased at high temperature, the thermal diffusivity of RHA shows a gradual decline with the increase of temperature from 25 to 300 °C. The thermal diffusivity behaviors of silica are consistent with the findings reported in the literature [10]. This phenomenon is obviously showed from the thermal diffusivity curves for crystalline silica samples (RHA-1000 °C to RHA-1400 °C). Their thermal diffusivities dropped more than 30% from 25 to 300 °C. The effect of phono-phonon scattering on the RHA-800 °C sample at high temperature is less significant because the motion of phonons in the sample is limited by its highly disorganized structure. Hence, the thermal diffusivity of the RHA-800 °C sample is more stable within the temperature range from 25 to 300 °C. The results indicate that the RHA-800 °C sample possesses excellent thermal insulation properties because it has the lowest and a steady thermal diffusivity over a broad range of temperatures compared to other RHA samples.

Conclusion

In this study, SiO_2-based ceramics with low thermal diffusivities were fabricated sintering of Malaysian rice husk at single temperature between 700 and 1400 °C. RHA produced by a sintering at 800 °C is rich in amorphous silica $(89.57 \pm 0.31 \text{ }wt.\%)$. The RHA-800 °C sample has a low density $(1.48 \pm 0.1 \text{ g cm}^{-3})$ and low thermal diffusivity $(0.17 \pm 0.1 \text{ mm}^2 \text{ s}^{-1})$. In addition, it has a stable thermal diffusivity at high temperatures. The product of sintering at 800 °C produced RHA which has desired thermal properties for thermal insulator application.

The crystalline phases in the RHA were identified using PXRD and FTIR. The results indicate the nucleation of *α*-cristobalite and *α*-tridymite took place at temperature between 800 and 900 °C, whereas the nucleation of *β*-tridymite took place at temperature between 1300 and 1400 °C. The FTIR measurements were extended to the far-infrared spectral range (400 to 280 cm^{-1}). Two far-infrared absorption bands (380 and 300 cm^{-1}) were observed from the FTIR spectra of RHA-1000 °C to RHA-1400 °C, correspond to the lattice vibrational modes of cristobalite. A complex particle surface fractal pattern was observed from the FESEM micrographs for the RHA-900 °C and RHA-1000 °C samples. The fractal pattern reflects the growth of *α*-cristobalite and *α*-tridymite crystals on the RHA particle surfaces. The RHA with *α*-cristobalite and *α*-tridymite phases (RHA-1000 °C to RHA-1400 °C) is composed of closely packed silica particles. They have higher bulk density and thermal diffusivity compared to amorphous RHA. Hence, they can be used as fire-resistant and fire extinguishing materials, instead of thermal insulating materials.

References

1. Kang, S.; Hong, S.; Moon, J.; *Cem. Concr. Res.*, **2019**, *115*, 389.
2. Sastré-Hernández, J.; Aguilar-Hernández, J.R.; Santoyo-Salazar, J.; Alfaro, H.M.; Hoyos-García, J.E.; Tufiño-Velázquez, M.; Contreras-Puente, G.; *Mater. Sci. Semicond. Process.*, **2020**, *114*, 105057.
3. Hossain, S.K.S.; Roy, P.K.; *J. Alloys Compd.*, **2020**, *817*, 152806.
4. Moayedi, H.; Aghei, B.; Abdullahi M.M.; Nguyen, H.; Rashid, A.S.A.; *J. Clean. Prod.*, **2019**, *237*, 117851.
5. Kim, Y.; Kim, Y.; Seo, W.; *J. Eur. Ceram.*, **2020**, *40 (7)*, 2623-2633.
6. Nuaklong, P.; Jongvivatsakul, P.; Posthisiri, T.; Sata, V.; Chindaprasirt, P.; *J. Clean. Prod.*, **2020**, *252*, 119797.
7. Malik, R.; Kim, Y.; Song, I.; *J. Eur. Ceram.*, **2020**, *40 (3)*, 594-602.
8. Mofid, S.A.; Jelle, B.P.; Zhao, X.; Gao, T.; Grandcolas, M.; Cunningham, B.; Ng, S.; Yang, R.; *J. Build. Eng.*, **2020**, *31*, 101336.
9. Rajpoot, S.; Malik, R.; Kim, Y.; *Ceram. Int.*, **2019**, *45*, 21270.
10. Hofmeister, A.M.; Whittington, A.G.; *J. Non. Cryst.*, **2012**, *358*, 1072.
11. Li, M.; Akoshima, M.; *Int. J. Heat Mass Transf.*, **2020**, *148*, 119017.
12. Coquard, R.; Baillis, D.; Grigorova, V.; Enguehard, F.; Quenard, D.; Levitz, P.; *J. Non. Cryst.*, **2013**, *363*, 103.
13. Sembiring, S.; Riyanto, A.; Rumiyanti, L.; Sembiring Z.; Situmeang, R.; *J. Aust. Ceram. Soc.*, **2020**, *56*, 433.
14. Mosina, K.S.; Nazarova, E.A.; Vinogradov, A.V.; Vinogradov, V.V.; Krivoshapkina, E.F.; Krivoshapkin, P.V.; *ACS Appl. Nano Mater.*, **2020**, *3*, 4386.
15. Sitarz, M.; Handke, M.; Mozgawa, W.; *Spectrochim. Acta. A.*, **2000**, *56*, 1819.

Authors biography

Dr Chee Wah Loy received his PhD in Advanced Materials Chemistry from The University of Sydney in 2018. Since 2010, he has been actively engaged in the fabrication and application research of nano and advanced materials, especially in the fields of biomedical and advanced manufacturing. He is currently an engineer at the Nano and Advanced Materials Institute, Hong Kong.